Vibrational Analysis of *trans*-Stilbene in the Ground and Excited Singlet Electronic States Revisited†

Hiroyuki Watanabe, Yuichi Okamoto, and Kazuhiko Furuya*,‡

Ashigara Research Laboratories, Fuji Photo Film Co. Ltd., 210 Nakanuma, Minami-Ashigara, Kanagawa 250-0193, Japan

Akira Sakamoto and Mitsuo Tasumi*

Department of Chemistry, Faculty of Science, Saitama University, Saitama 338-8570, Japan

Received: August 27, 2001

The Raman and infrared bands of *trans*-stilbene in the ground electronic state (S_0) and an excited singlet state (S_1) are assigned on the basis of density functional calculations at the 6-311+G** level for the S_0 state and configuration interaction single calculations with the 6-311+G** basis set for the S_1 state. Not only the wavenumbers of normal modes but also Raman activities, Raman depolarization ratios, and infrared intensities are calculated and used for band assignments. The vibrational patterns of some characteristic modes are discussed. It is found that, with respect to a few low-wavenumber modes in both the S_0 and S_1 states, the results of the present calculations are inconsistent with those derived from an analysis of the fluorescence excitation spectra and dispersed fluorescence spectra of *trans*-stilbene in a supersonic jet.

1. Introduction

The molecular structure and spectra of *trans*-stilbene (tSB) in the ground electronic state (S_0) have been studied from various viewpoints by many authors. The vibrational (infrared and Raman) spectra of tSB and its isotopic analogues in the S_0 state have been reported in considerable detail,[1−3] and band assignments have also been performed on the basis of normal coordinate calculations at various levels.[2−7] The first aim of the present study is to establish definitive assignments of the infrared and Raman bands of tSB in the S_0 state by performing up-to-date density functional calculations with a large set of basis functions.

The Raman spectrum of tSB in an excited singlet electronic state (which is called the S_1 state according to the traditional naming) was first reported in 1983.[8,9] Since then, numerous studies have been published on this subject.[6,10−24] More recently, the infrared spectrum of tSB in the S_1 state was also observed.[25,26] Although normal coordinate analyses of tSB in the S_1 state based on an empirical force field[6] and extended Hückel calculations[14] have been performed to assign the observed Raman bands, no attempt to derive the vibrational wavenumbers and modes of tSB in the S_1 state from ab initio molecular orbital calculations at a high level has been reported so far. The second aim of the present study is to make an effort to analyze the observed Raman and infrared spectra of tSB in the S_1 state by performing molecular orbital calculations using the configuration interaction singles (CIS) method,[27] which was useful in the analysis of the resonance Raman excitation profiles of all-*trans*-hexatriene.[28]

2. Experimental and Computational Procedures

In the present study, the following infrared and Raman spectra of tSB at 1 cm^{-1} resolution were observed to examine the reliability of the previously reported spectral data as well as to obtain some new information: (1) the infrared spectra in *n*-hexane and benzene solutions in the region of 1800−450 cm^{-1}, with solvent bands being carefully subtracted; (2) the infrared spectrum in KBr disk in the region of 1800−100 cm^{-1}; (3) the Raman spectra in *n*-hexane and benzene solutions in the region of 1800−200 cm^{-1}, with careful subtraction of solvent bands; (4) the Raman spectrum in powder in the region of 1800−200 cm^{-1}; (5) the polarized and depolarized Raman spectra in benzene solution in the region of 1800−100 cm^{-1}.

Infrared spectra in the region of 1800−450 cm^{-1} were recorded on a BIO-RAD FTS-40 Fourier transform infrared spectrometer, and far-infrared spectra in the region of 600−100 cm^{-1} on a Bruker IFS 66v/S Fourier transform spectrometer. Raman spectral measurements were performed with a Bruker RFS-100 Fourier transform Raman spectrometer by using Nd:YAG 1064-nm light for Raman excitation.

Molecular structural parameters, vibrational wavenumbers, vibrational modes, Raman activities, Raman depolarization ratios, and infrared intensities of tSB in the S_0 state were calculated by using the B3LYP functional[29,30] in combination with the 6-311+G** basis set. Molecular structural parameters, vibrational wavenumbers, vibrational modes, and infrared absorption intensities of tSB in the S_1 state were calculated by the CIS method[27] using the 6-311+G** basis set. The Gaussian 98 revision A.9 program package[31] was used at a network parallel excursion mode with Linda (embedded in Gaussian 98) on two computer systems, namely, an HPC Alpha 21264 (500 MHz × 4 CPU) and an HPC Alpha 21164 (600 MHz × 4 CPU).

† Part of the special issue "Mitsuo Tasumi Festschrift".

* Corresponding authors.

‡ Telephone: +81-465-73-7080. Facsimile: +81-465-73-7923. E-mail: kazuhiko_furuya@fujifilm.co.jp

10.1021/jp013309t CCC: $22.00
Published on Web 01/19/2002

TABLE 1: Lengths of the CC Bonds in the S_0 and S_1 States of tSB under C_{2h} Symmetry

	bond length/Å			
	S_0		S_1	
bond	B3LYP[a]	X-ray[b]	CIS[a]	Δr r(CIS) − r(B3LYP)
$r(C_\alpha C_{\alpha'})$	1.345	1.326	1.409	+0.064
$r(C_\alpha C_1)$	1.466	1.471	1.407	−0.059
$r(C_1C_2)$	1.407	1.397	1.429	+0.022
$r(C_2C_3)$	1.389	1.381	1.378	−0.011
$r(C_3C_4)$	1.397	1.383	1.388	−0.009
$r(C_4C_5)$	1.393	1.381	1.405	+0.012
$r(C_5C_6)$	1.392	1.384	1.365	−0.027
$r(C_6C_1)$	1.406	1.392	1.427	+0.021

[a] The basis set used is 6-311+G**. [b] Reference 33.

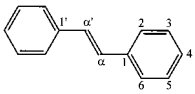

Figure 1. Molecular structure of tSB and carbon numbering.

Calculated vibrational modes were depicted by the use of the LXVIEW program.[32]

3. Results and Discussion

A. Molecular Structure of tSB in the S_0 State. The molecular geometry of tSB in the S_0 state was fully optimized under C_{2h} symmetry at the B3LYP/6-311+G** level. The fact that no imaginary value was obtained in the calculation of vibrational wavenumbers supports the planarity of tSB in the S_0 state. In Table 1, the calculated CC bond lengths are compared with the values obtained from an X-ray analysis.[33] The calculated bond lengths agree with the corresponding X-ray values with deviations smaller than 0.02 Å. The calculated structural parameters can safely be used for the calculation of vibrational wavenumbers, modes, Raman activities, Raman depolarization ratios, and infrared intensities.

B. Vibrational Analysis of tSB in the S_0 State. All the results of calculations peformed for tSB in the S_0 state are given in Table 2 and Figure 2, except for the results relating to the CH stretching modes having wavenumbers higher than 3000 cm^{-1}. In the present paper, attention is focused on the other modes with wavenumbers lower than 1700 cm^{-1}, which are more interesting from the viewpoint of vibrational spectroscopy. Since tSB consists of 26 atoms and has C_{2h} symmetry, its 72 normal modes are classified into the a_g, a_u, b_g, and b_u species, i.e., 25 modes ($\nu_1 - \nu_{25}$) in a_g, 12 modes ($\nu_{26} - \nu_{37}$) in a_u, 11 modes ($\nu_{38} - \nu_{48}$) in b_g, and 24 modes ($\nu_{49} - \nu_{72}$) in b_u. Among them, six modes ($\nu_1 - \nu_6$) in a_g and six modes ($\nu_{49} - \nu_{54}$) in b_u are the CH stretches. Therefore, these 12 modes are omitted in Table 2 and Figure 2. In view of the overall reliability of the calculated results presently obtained for tSB, which is an important molecule in physical chemistry, the patterns of all the normal modes except for the twelve CH stretches are depicted in Figure 2. The visualization of normal modes is an easy way for understanding their characters.

In the following part of this section it is shown that definitive assignments of the infrared and Raman bands of tSB observed in the 1700−300 cm^{-1} region are obtained on the basis of the present calculations, and it is also pointed out that some inconsistencies in band assignments exist for modes below 300 cm^{-1} between the present calculations and analyses[34,35] of the fluorescence excitation spectra and dispersed fluorescence spectra of tSB in the supersonic jet as well as vapor-phase

TABLE 2: Calculated and Observed Vibrational Wavenumbers, Raman and Infrared Intensities, and Raman Depolarization Ratios for tSB in the S_0 State

		calculated[a]			observed[b]		
symmetry species	mode	ν/cm^{-1}	intensity	DP	ν/cm^{-1}	intensity	DP
a_g	ν_7	1649	3211.4	0.32	1639	vs	0.30
	ν_8	1598	4158.7	0.37	1600	vs	0.41
	ν_9	1575	317.4	0.36	1577	w	0.37
	ν_{10}	1489	258.2	0.37	1492	w	0.35
	ν_{11}	1443	198.4	0.36	1448	w	0.32
	ν_{12}	1336	500.3	0.30	1336	w	0.26
	ν_{13}	1321	237.8	0.33	1320	w	0.26
	ν_{14}	1300	66.4	0.39	1293[c]	vw	0.39
	ν_{15}	1185	774.3	0.30	1194	s	0.27
	ν_{16}	1180	956.6	0.28	1183	w	0.22
	ν_{17}	1158	28.0	0.74	1157	vw	0.72
	ν_{18}	1081	3.0	0.15	−	−	−
	ν_{19}	1025	74.0	0.10	1028	w	0.08
	ν_{20}	991	414.6	0.19	1001	s	∼0.1
	ν_{21}	862	22.7	0.72	869	vw	0.42
	ν_{22}	641	6.0	0.12	641	vw	0.13
	ν_{23}	619	19.3	0.64	620	vw	0.68
	ν_{24}	282	1.6	0.53	291[d]	vw	−
	ν_{25}	201	2.2	0.25	203[d]	vw	−
a_u	ν_{26}	983	10.7	−	980	w	−
	ν_{27}	967	29.8	−	959	s	−
	ν_{28}	961	0.5	−	−	−	−
	ν_{29}	902	1.1	−	907	vw	−
	ν_{30}	829	0.3	−	−	−	−
	ν_{31}	762	72.1	−	760	vs	−
	ν_{32}	686	83.2	−	691	vs	−
	ν_{33}	531	20.6	−	526	m	−
	ν_{34}	400	0.0	−	408[e]	vw	−
	ν_{35}	281	0.0	−	286[e]	vw	−
	ν_{36}	58	0.5	−	−	−	−
	ν_{37}	11	0.0	−	−	−	−
b_g	ν_{38}	979	3.3	0.75	985[f]	−	−
	ν_{39}	962	0.1	0.75	969[f]	−	−
	ν_{40}	915	6.4	0.75	914[c]	vw	−
	ν_{41}	864	25.8	0.75	848	vw	0.69
	ν_{42}	828	3.3	0.75	821	vw	0.59
	ν_{43}	734	2.1	0.75	736[c]	vw	−
	ν_{44}	683	0.0	0.75	−	−	−
	ν_{45}	466	0.2	0.75	464[d]	vw	−
	ν_{46}	403	0.1	0.75	406[d]	vw	∼0.6
	ν_{47}	220	7.1	0.75	227	w	0.66
	ν_{48}	82	0.5	0.75	−	−	−
b_u	ν_{55}	1607	25.4	−	1603	w	−
	ν_{56}	1581	3.0	−	1581	vw	−
	ν_{57}	1497	29.0	−	1497	w	−
	ν_{58}	1451	10.1	−	1453	w	−
	ν_{59}	1342	4.5	−	1337	vw	−
	ν_{60}	1326	2.6	−	1327	vw	−
	ν_{61}	1262	1.5	−	1262	w	−
	ν_{62}	1224	1.8	−	1214	vw	−
	ν_{63}	1178	0.2	−	1179	vw	−
	ν_{64}	1157	0.4	−	1155	vw	−
	ν_{65}	1079	11.3	−	1071	w	−
	ν_{66}	1027	7.6	−	1031	w	−
	ν_{67}	992	0.1	−	−	−	−
	ν_{68}	815	2.1	−	−	−	−
	ν_{69}	622	0.0	−	−	−	−
	ν_{70}	540	20.3	−	538	w	−
	ν_{71}	463	2.2	−	469[e]	w	−
	ν_{72}	79	0.2	−	−	−	−

[a] Wavenumbers scaled by a single factor of 0.9785 are given. Raman activities calculated for the a_g and b_g modes are given in units of $Å^4$ amu^{-1}, and infrared intensities calculated for the a_u and b_u modes in units of km mol^{-1}. DP stands for the Raman depolarization ratio. [b] Wavenumbers and intensities observed in *n*-hexane solution and DP values observed in benzene solution are given unless otherwise noted. [c] Observed in benzene solution. [d] Observed in powder. [e] Observed in powder in polyethylene. [f] Based on an analysis of combination bands (ref 36).

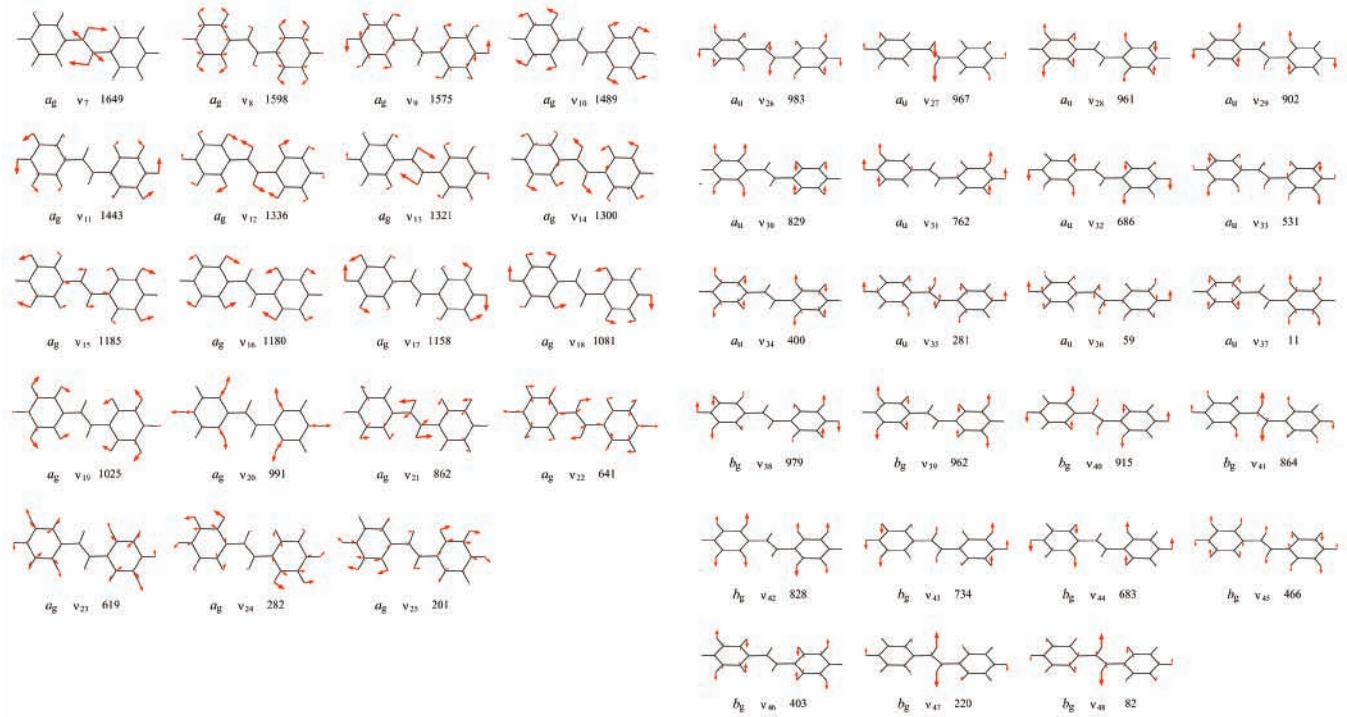

Figure 2. Vibrational patterns of the normal modes of tSB in the S_0 state (except for the CH stretches). The symmetry species, mode number, and scaled wavenumber are given to each mode.

Raman data at 330 °C. Detailed comparisons of the present band assignments with those derived from the previous normal-coordinate analyses[2−7] are not presented, because it is natural to consider (at least as far as the modes with wavenumbers higher than 300 cm^{-1} are concerned) that the present calculations (performed at a strong theoretical basis and giving not only the vibrational wavenumbers and patterns but also the infrared intensities, Raman activities, and Raman depolarization ratios) are much more informative and reliable than the previous normal-coordinate analyses, which were based upon either "experimental" force fields or molecular-orbital calculations at levels not so high as the level employed in the present calculations. This does not mean, however, that the previous studies had many misassignments. Rather, the present calculations have confirmed that the previous assignments of important bands were largely correct.

The calculated vibrational wavenumbers were multiplied by a single scale factor of 0.9785 to obtain a good fit between the calculated and observed wavenumbers in the 1700−300 cm^{-1} region. The scaled wavenumbers are given in Table 2 as the calculated wavenumbers. The agreement between the calculated and observed wavenumbers is surprisingly good; the differences between them are smaller than 10 cm^{-1} with the single exception of ν_{41} in b_g, for which the difference is 16 cm^{-1}. Bands usually observed in the Raman and infrared spectra of tSB in the 1700−300 cm^{-1} region are satisfactorily assigned in Table 2, and only extremely weak bands are left unassigned. In Table 2, the wavenumbers of the Raman and infrared bands observed in *n*-hexane solution are given when available, since hardly any specific intermolecular interaction exist between tSB and *n*-hexane. If necessary data are not available in *n*-hexane solution because of overlapping of bands due to tSB and *n*-hexane or a low solubility of tSB in *n*-hexane, data obtained in either benzene solution or in powder are used. Only for ν_{38} and ν_{39} are the wavenumbers obtained from an analysis of the combination bands[36] used, because it is not possible to observe them directly. The above-mentioned deviation of the calculated wavenumbr of ν_{41} (864 cm^{-1}) from the observed wavenumber (848 cm^{-1}) may be related to the fact that there are two closely located modes, ν_{41} and ν_{42}, in the same b_g species. As shown in Figure 2, ν_{41} is an ethylenic CH out-of-plane bend and ν_{42} is a ring CH out-of-plane bend. It is possible that the calculated results do not correctly reflect the existing interaction (or nonexistence of interaction) between the two modes.

As shown in Table 2, the calculated Raman activities (which should be proportional to the observed Raman intensities), Raman depolarization ratios, and infrared intensities are broadly in agreement with the observed data. The very large Raman activities calculated for ν_7 and ν_8 explain the very strong intensities of the two Raman bands at 1639 and 1600 cm^{-1}, respectively. Similarly, the large Raman activities are calculated for ν_{15} and ν_{20}, to which the strong Raman bands at 1194 and 1001 cm^{-1} are assigned, respectively. However, some discrepancies between the calculated Raman activities and the observed Raman intensities are found for ν_{12} and ν_{16}; the weak Raman bands at 1336 and 1183 cm^{-1} are assigned, respectively, to ν_{12} and ν_{16}, while the Raman activities calculated for these modes (particularly ν_{16}) are large. This discrepancy for ν_{16} may be associated with the presence of ν_{15} at a position very close to ν_{16}. The interaction between ν_{15} and ν_{16} may not be correctly expressed in the calculated results; ν_{15} should actually have a larger Raman activity and ν_{16} a smaller value. The weaker Raman intensities of the other observed a_g bands are mostly explained by the smaller Raman activities calculated for them. The Raman activities calculated for the b_g modes are generally small, and these small values are consistent with the very weak Raman intensities of the observed b_g bands.

The vibrational patterns of a few a_g modes with strong Raman intensities may be worthy of notice. As shown in Figure 2, ν_7 is the ethylenic $C_\alpha C_{\alpha'}$ stretch coupled with the ethylenic CH symmetric in-plane bend, and ν_8 is primarily a ring CC stretch with a minor contribution from the ethylenic $C_\alpha C_{\alpha'}$ stretch and the $C_\alpha C_1$ and $C_{\alpha'} C_{1'}$ symmetric stretch. In ν_{15}, the $C_\alpha C_1$ and $C_{\alpha'} C_{1'}$ symmetric stretch is coupled with a ring CH bend. This

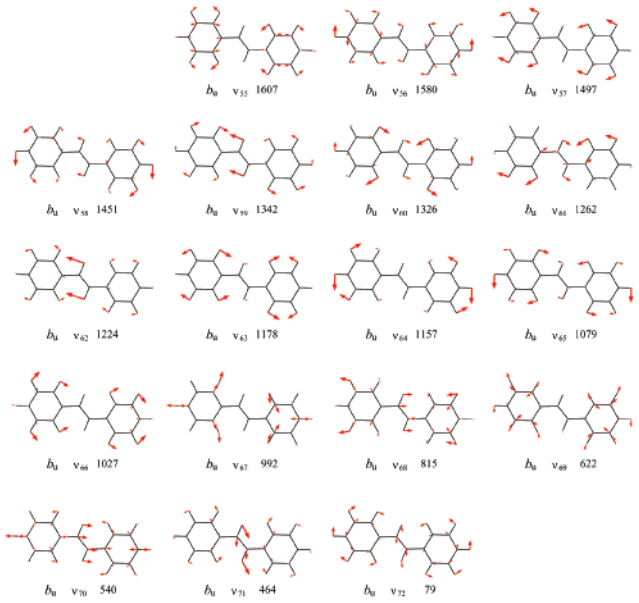

Figure 2 (continued).

ring CH bend, which greatly contributes to ν_{16}, seems to have a large intrinsic Raman activity according to the results of calculations. The strong Raman band at 1001 cm^{-1} is assigned to ν_{20}, which is called the "trigonal" ring CC stretch corresponding to a transformation of a hexagon into a triangle. Because of the band position at 1001 cm^{-1}, this band is often mistakenly assigned to the breathing vibration, which gives rise to a strong Raman band at 992 cm^{-1} in the case of benzene. It should be emphasized that tSB does not have a genuine ring breathing mode. In other words, it is not a good practice to discuss the normal modes of tSB by analogy with those of benzene. As pointed out earlier in the case of toluene,[37] similarities between the normal modes of a monosubstituted benzene and those of benzene are not always guaranteed.

As given in Table 2, the Raman depolarization ratios (DPs) calculated for the a_g modes are generally in agreement with the observed. The DPs calculated for most modes in a_g are smaller than 0.4 and are consistent with the observed data. Exceptions are ν_{17}, ν_{21}, and ν_{23}, for which the calculated DPs are larger than 0.6. The DP calculated for ν_{17} is as large as 0.74, although ν_{17} (ring CH bend) is a totally symmetric mode in a_g. It is interesting to note that, in fact, the DP observed for the Raman band at 1157 cm^{-1} assigned to ν_{17} is 0.72. Similarly, the DP calculated for ν_{23} (ring deformation) is 0.64, which is close to the value (0.68) observed for the Raman band at 620 cm^{-1} assigned to ν_{23}. Only for ν_{21} (ethylenic part deformation), is a clear discrepancy between the calculated and observed DPs found; the observed DP (0.42) of the Raman band at 869 cm^{-1} assigned to ν_{21} is considerably smaller than the calculated DP (0.72) for ν_{21}. The DPs observed for ν_{41}, ν_{42}, ν_{46}, and ν_{47} in b_g are larger than about 0.6 but smaller than the theoretically expected values for the b_g modes (0.75). This discrepancy is due either to experimental difficulties in determining accurately the DPs of very weak bands or to a deviation of the molecular structure in solution from the planar form.[38,39] The latter point will be discussed in a separate paper.[40]

The infrared spectrum of tSB does not have strong bands in the region of 1700−1000 cm^{-1}. All the bands observed in this region are due to the b_u modes, for which the calculated infrared intensities are generally small except for those of ν_{55} (ring CC stretch) and ν_{57} (ring CH bend). The medium-intensity to very strong infrared bands are observed in the region of 1000−500 cm^{-1}, and they are assigned to the following four CH out-of-plane wags in a_u: ν_{27} (in-phase ethylenic CH wag), ν_{31} (ring CH wag), ν_{32} (ring CH wag), and ν_{33} (ring CH wag). The infrared intensities calculated for these four modes satisfactorily account for the observed relative intensities of the four bands at 959, 760, 691, and 526 cm^{-1}, respectively.

Many modes in a_g have their counterparts in b_u; ν_i in a_g and ν_{i+47} in b_u often make a pair. The ν_i and ν_{i+47} modes are symmetric and antisymmetric, respectively, with respect to the vibrational displacements in the left and right halves of the molecule. In Figure 2, ν_i and ν_{i+47} are placed in the corresponding positions in the panels for a_g and b_u for convenience of comparison. The modes in pairs are close in their wavenumbers. For example, the wavenumber of ν_{10} is 1489 cm^{-1}, while that of ν_{57} is 1497 cm^{-1}. Some exceptions to the ν_i and ν_{i+47} pair exist; ν_{14} and ν_{15} are related to ν_{61} and ν_{62} in pairs, and ν_{22} makes a pair with ν_{70} rather than with ν_{69} (ν_{23} makes a pair with ν_{69}). The low-wavenumber modes ν_{24} and ν_{25} are far from ν_{71} and ν_{72} in their vibrational patterns as well as in their wavenumbers.

As described above, the present calculations explain the observed infrared and Raman bands observed in the 1700−300 cm^{-1} region to a satisfactory degree, although some deviations of the calculated values from the observed Raman intensities (activities) and depolarization ratios exist for a few Raman bands. On the contrary, as mentioned earlier, the results of the present calculations and measurements are inconsistent, with respect to a few modes in the region below 300 cm^{-1}, with band assignments derived from the latest analyses[34,35] of the fluorescence excitation spectra and dispersed fluorescence spectra of tSB in the supersonic and the Raman spectrum of tSB in the vapor phase at 330 °C. Eight modes (ν_{24} and ν_{25} in a_g; ν_{35}, ν_{36}, and ν_{37} in a_u; ν_{47} and ν_{48} in b_g; ν_{72} in b_u) are expected to exist in the region below 300 cm^{-1}. Among these, the wavenumber values taken for ν_{24}, ν_{36}, ν_{37}, ν_{47}, and ν_{72} by Laane and co-workers[34,35] are, respectively, 273, 58, 8[34] (9[35]), 211, and 76. These values are close to those taken in the present study (Table 2). Serious disagreements between Laane et al. and the present study exist with respect to the wavenumber values taken for ν_{25}, ν_{35}, and ν_{48}, which are, respectively, 152, 101, and 118 cm^{-1} according to Laane et al. and 203, 286, and 82 cm^{-1} (only 82 cm^{-1} being the calculated value) in the present study. The assignments given in the present study are of course consistent with the results of calculations (Table 2), and they are also largely in line with the assignments[41−44] reported before the studies by Laane et al.

In the Raman spectrum of tSB in the vapor phase at 330 °C, a strong polarized band was observed at 152 cm^{-1} by Laane et al.[35] However, no such band is observed in the Raman spectrum of powder tSB, which clearly shows only three bands at 291, 229, and 203 cm^{-1} in the 300−100 cm^{-1} region, the 229-cm^{-1} band being much stronger than the other two. Therefore, the assignment of the 152-cm^{-1} Raman band to ν_{25} cannot be supported, although the origin of this band remains to be solved. The discrepancy between Laane et al. and the present study is even more striking for ν_{35}. In the framework of the present molecular orbital or density functional calculations, it is most unlikely to have the calculated wavenumber for ν_{35} in the region around 100 cm^{-1} instead of 286 cm^{-1} obtained in the present calculations. The large discrepancy between the calculated wavenumber for ν_{35} and the wavenumber (101 cm^{-1}) derived from the fluorescence analysis[34] (which is the latest on this subject and seems to be thorough) remains to be puzzling at present.

C. Molecular Structure of tSB in the S_1 State. The lowest excited singlet state (S_1) calculated by the CIS method has a

simple configuration derived from the HOMO−LUMO transition, with an energy of 3.80 eV above the ground state (S_0). In Table 1, the lengths of the CC bonds in the optimized geometry of tSB in the S_1 state are compared with those in the S_0 state. Clearly, major structural changes on going from S_0 to S_1 occur in the ethylenic part.

The above picture of the lowest excited singlet state obtained by the CIS method is considerably different from the results reported by Molina et al.[45] using multiconfigurational second-order perturbation theory (CASPT2). According to their calculations, there are two optically allowed, low-lying excited singlet states: 1^1B_u (3.77 eV) and 2^1B_u (4.07 eV). The second lowest 2^1B_u state (which should be called S_2), rather than the lowest 1^1B_u state, bears a certain similarity to the CIS-derived S_1 state, but the CASPT2-derived S_2 state has a more complex character consisting of various configurations.

Although the picture of the CIS-derived S_1 state may be too simple, the vibrational wavenumbers, modes, and the infrared intensities (for the a_u and b_u modes) of tSB in the S_1 state were calculated by the use of the molecular structural parameters and force constants obtained by the CIS method, as an initial step toward the vibrational analysis of large molecules in excited electronic states based on ab initio molecular orbital calculations at high levels.

D. Vibrational Analysis of tSB in the S_1 State. The results of calculations are given in Table 3, together with the observed data. The wavenumbers in Table 3 are scaled by a single factor of 0.9129. Since all the Raman and infrared bands observed so far are assignable to modes in a_g (Raman) and b_u (infrared), the results of calculations for the a_u and b_g species are not listed in Table 3. The Raman spectrum of tSB in the S_1 state was observed in resonance with the $S_n \leftarrow S_1$ absorption. It is not possible at present to calculate the Raman activities to be compared with the observed Raman intensities. However, it is not difficult to find correspondences between the calculated modes and the observed Raman bands by reference to the calculated and observed shifts on going from the normal species to the α,α'-^{13}C-substituted species. The Raman bands showing ^{13}C downshifts greater than 5 cm^{-1} are those at 1566 (−21), 1534 (about −10), 1241 (−5), 1179 (−11), 1148 (−5), and 844 (−10) cm^{-1} (downshifts are given in parentheses).[12] These downshifts correspond, respectively, to those calculated for ν_8 (−15), ν_9 (−7), ν_{14} (−6), ν_{16} (−14), ν_{17} (−2), and ν_{21} (−10). The ^{13}C downshifts of the other bands are smaller than 3 cm^{-1}, and such results agree with the calculated. For example, the calculated wavenumber of ν_{15} of the ^{13}C species is 1179 cm^{-1}, which is the same as that of the normal species given in Table 3. Therefore, the observed 1179 cm^{-1} band, which shows a ^{13}C downshift of 11 cm^{-1}, cannot be assigned to ν_{15}, although it is tempting to assign this band to ν_{15} and the 1148 cm^{-1} band to ν_{16} in view of the proximity of the calculated and observed wavenumbers.

Comparisons of the vibrational patterns in the S_0 and S_1 states indicate that the vibrational patterns of many modes in a_g and b_u do not change greatly between S_0 and S_1. In a_g, the vibrational patterns of ν_7, ν_8, ν_{14}, and ν_{16} in S_1 shown in Figure 3 are considerably different from ν_7, ν_8, ν_{14}, and ν_{15} (not ν_{16}) in S_0 (ν_{16} in S_0 is close to ν_{15} in S_1). All the pertinent modes have contributions from atomic displacements in the ethylenic part. The structural changes occurring in the ethylenic part on going from S_0 to S_1 cause the above-mentioned differences in the corresponding modes between S_0 and S_1.

The spectral changes in the 1700−1000 cm^{-1} region on going from S_0 to S_1 seem to be associated with the degrees of contributions of the $C_\alpha C_{\alpha'}$ stretch to the modes in S_1, although it is not possible to discuss this point quantitatively. In fact, ν_8, ν_{14}, and ν_{16} in S_1 have significant contributions of the $C_\alpha C_{\alpha'}$ stretch (see Figure 3). Similarly, major spectral changes in S_1 upon ^{13}C substitution are also associated with changes in the contributions of the $C_\alpha C_{\alpha'}$ stretch to the pertinent modes. The spectral changes in S_1 occurring in the 1600−1500 cm^{-1} region upon ^{13}C substitution can be explained by mode rearrangements in ν_8 and ν_9; ν_9 of the ^{13}C species has a larger contribution of the $C_\alpha C_{\alpha'}$ stretch than ν_9 of the normal species. Similarly, the spectral changes in S_1 in the 1200−1100 cm^{-1} region upon ^{13}C substitution seem to be associated with a mode rearrangement in ν_{17}. The vibrational patterns of ν_{17} of the normal species

TABLE 3: Calculated and Observed Vibrational Wavenumbers and Raman and Infrared Intensities for tSB in the S_1 State

symmetry species	mode	calculated[a,b,c] ν/cm^{-1}	calculated[a,b,c] intensity	observed[d,e] ν/cm^{-1}	observed[d,e] intensity
a_g	ν_7	1633	−	−	−
	ν_8	1561	−	1566	m
	ν_9	1535	−	1534	w
	ν_{10}	1469	−	1458	w
	ν_{11}	1431	−	1421	w
	ν_{12}	1343	−	1331	w
	ν_{13}	1285	−	−	−
	ν_{14}	1237	−	1241	m
	ν_{15}	1179	−	−	−
	ν_{16}	1155	−	1179	s
	ν_{17}	1128	−	1148	m
	ν_{18}	1074	−	1077	w
	ν_{19}	994	−	−	−
	ν_{20}	970	−	978	w
	ν_{21}	842	−	844	m
	ν_{22}	621	−	620	w
	ν_{23}	598	−	−	−
	ν_{24}	279	−	285	s
	ν_{25}	201	−	197	w
b_u	ν_{55}	1580	4.9	∼1570(*a*)	w
	ν_{56}	1529	18.7	∼1540(*h*,*a*)	w
	ν_{57}	1474	32.6	∼1500(*h*,*a*)	m
	ν_{58}	1445	13.8	∼1400(*h*)	m
	ν_{59}	1354	3.2	1343(*h*)	w
				1347(*a*)	w
	ν_{60}	1300	9.8	1289(*h*)	w
				1280(*a*)	w
	ν_{61}	1282	6.3	1253(*a*)	w
	ν_{62}	1200	11.2	1215(*h*)	m
				1215(*a*)	w
	ν_{63}	1160	5.0	1179(*a*)	w
	ν_{64}	1126	7.6	1145(*h*)	s
				1148(*a*)	s
	ν_{66}	995	7.2	−	
	ν_{67}	952	58.3	960(*h*,*a*)	vs
	ν_{68}	790	2.5	−	−
	ν_{69}	605	2.2	−	−
	ν_{70}	520	22.8	−	−
	ν_{71}	463	2.3	−	−
	ν_{72}	83	0.0	−	−

[a] Wavenumbers scaled by a single factor of 0.9129 are given. Raman intensities for the a_g mode are not calculated. Infrared intensities calculated for the b_u modes are given in units of km mol^{-1}. [b] Wavenumbers and infrared intensities calculated for the a_u modes are (intensities in parentheses) ν_{26} 995 (0.0), ν_{27} 988 (0.0), ν_{28} 895 (10.5), ν_{29} 821 (50.9), ν_{30} 787 (40.5), ν_{31} 747 (50.5), ν_{32} 650 (125.7), ν_{33} 480 (28.8), ν_{34} 402 (0.2), ν_{35} 210 (0.6), ν_{36} 48 (0.5), and ν_{37} 19 (0.0). [c] Wavenumbers calculated for the b_g modes are ν_{38} 995, ν_{39} 988, ν_{40} 892, ν_{41} 826, ν_{42} 794, ν_{43} 724, ν_{44} 643, ν_{45} 443, ν_{46} 410, ν_{47} 274, and ν_{48} 118. [d] Observed Raman data for the a_g modes are those taken in *n*-hexane solution in refs 10−12. [e] Observed infrared data for the b_u modes are those taken in *n*-heptane solution (indicated as *h*) and acetonitrile solution (indicated as *a*) in ref 26.

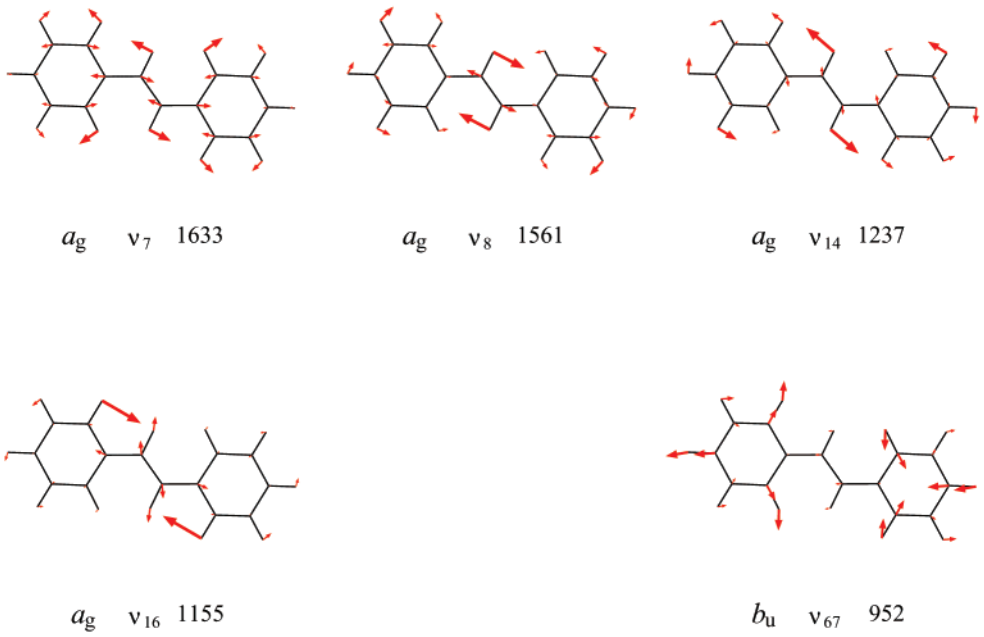

Figure 3. Vibrational patterns of some normal modes of tSB in the S_1 state. The symmetry species, mode number, and scaled wavenumber are given to each mode.

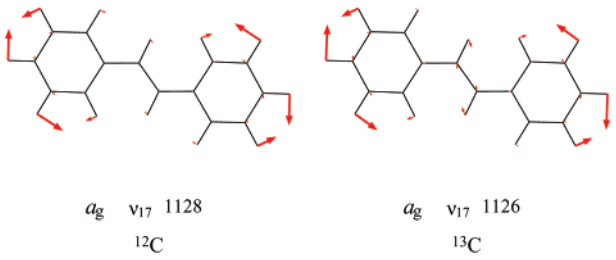

Figure 4. Vibrational patterns of ν_{17} of the normal (^{12}C) and α,α′-^{13}C-substituted tSB in the S_1 state. The symmetry species, mode number, and scaled wavenumber are given to each mode.

and that of the ^{13}C species in S_1 are compared in Figure 4. It is clear that ν_{17} of the ^{13}C species has a contribution of the $C_\alpha C_{\alpha'}$ stretch, while ν_{17} of the normal species has no such contribution. Most probably, this difference gives a much higher intensity to the 1145 cm^{-1} band of the ^{13}C species as compared with the weak intensity of the 1150 cm^{-1} band of the normal species. (The wavenumber readings, 1145 and 1150 cm^{-1}, are taken from ref 12. The 1150 cm^{-1} band in ref 12 correspond to the 1148 cm^{-1} band in Table 3.)

The intensities of the S_1 Raman bands in the region below 1000 cm^{-1} are not associated with the contributions of the $C_\alpha C_{\alpha'}$ stretch. No correlation seems to exist between the intensity of an S_1 Raman band and that of the corresponding S_0 Raman band. For example, the medium-intensity band at 844 cm^{-1} is assigned to ν_{21}, whose vibrational pattern is close to that of ν_{21} in S_0. The corresponding band at 869 cm^{-1} in the S_0 Raman spectrum is very weak in intensity. The strong S_1 Raman band at 285 cm^{-1} is assigned to ν_{24}, whose vibrational pattern is unchanged from that of ν_{24} in S_0. The corresponding band at 291 cm^{-1} in the S_0 Raman spectrum is so weak that it can be observed only in the powder sample. The observed medium to strong Raman intensities of ν_{21} and ν_{24} in S_1 may be related to the molecular structure of tSB in the S_n state, giving rise to the $S_n \leftarrow S_1$ absorption.

As shown in Table 3, the observed S_1 infrared bands[24,25] can be assigned to the calculated modes in b_u without difficulty. However, the agreement between the calculated and observed wavenumbers is less satisfactory than that between the S_1 Raman bands and the calculated modes in a_g. This is partly because the observed peak wavenumbers are not accurately determined due to experimental difficulties. The results of calculations are particularly helpful in clarifying the origin of the very strong S_1 infrared band at 960 cm^{-1}. This band is assigned to ν_{67} whose vibrational pattern is shown in Figure 3. In fact, the infrared intensity calculated for ν_{67} in S_1 is very large. In ν_{67} in S_1, the trigonal ring stretch in one phenyl ring is coupled out-of-phase with the same mode in the other phenyl ring. The vibrational pattern of ν_{67} in S_1 is essentially the same as that of ν_{67} in S_0, as shown in Figures 2 and 3. Nonetheless, the infrared intensity calculated for ν_{67} in S_0 is very weak (about 1/580 of the infrared intensity calculated for ν_{67} in S_1). This result indicates that, in the S_1 state, the positive and negative charges move back and forth between the two phenyl rings of tSB synchronously with the vibration of ν_{67}, whereas such molecular-vibration-induced dipole oscillation does not occur in the S_0 state.

Okamoto reported[25] that the S_1 infrared spectrum observed in acetonitrile solution was slightly different from that observed in *n*-heptane solution; a few bands were additionally observed in acetonirile solution. It was suggested[25] that the bands additionally observed in acetonitrile solution might be due to Raman-active a_g modes activated in the infrared spectrum by interactions between tSB and polar acetonitrile molecules. This is an interesting view, but it is worth noticing that, as given in Table 3, not only the infrared bands observed in *n*-heptane solution but also the bands additionally observed in acetonitrile solution are reasonably assigned to modes in b_u. It is interesting to note that the infrared intensities calculated for the S_1 modes in the 1300−1100 cm^{-1} region are much higher than those calculated for the corresponding S_0 modes (see Tables 2 and 3).

With respect to a few modes with wavenumbers lower than 300 cm^{-1}, the calculated wavenumbers do not agree with the values derived from the fluorescence analysis.[34] The wavenum-

bers calculated (scaled by a factor of 0.9129) for ν_{35}, ν_{36}, and ν_{37} in a_u are 210, 48, and 19 cm^{-1}, respectively, whereas the values derived from the fluorescence analysis are 99, 47.5, and 35 cm^{-1}, respectively. The situation that the discrepancy for ν_{35} is particularly large is similar to the S_0 case described earlier. The wavenumbers calculated for ν_{47} and ν_{48} in b_g are 274 and 118 cm^{-1}, respectively. The latter value is much higher than the calculated wavenumber (82 cm^{-1}) of ν_{48} in S_0, and agrees reasonably with the value (110 cm^{-1}) derived from the fluorescence analysis.

4. Concluding Remarks

The first aim of this study was to establish definitive assignments of the observed Raman and infrared bands of tSB in the ground electronic state on the basis of density functional calculations using a large basis set. This aim has been achieved to a satisfactory degree as far as the infrared and Raman bands observed in the 1700−300 cm^{-1} region are concerned.

Studies toward the second aim of making a spectral analysis of tSB in an excited singlet state with the help of ab initio molecular orbital calculations at a high level have proved that the configuration interaction singles (CIS) method is very useful for the analysis of the observed Raman and infrared spectra of tSB in the excited singlet state. Whether the CIS-derived simple picture of the excited singlet state is true or not may be a problem to be studied further. However, the vibrational wavenumbers, modes, and infrared intensities calculated by this method convincingly account for the observed Raman bands in the 1600−100 cm^{-1} region and infrared bands in the 1600−900 cm^{-1} region.

It has been also found that the results of the present calculations for a few modes in the region below 300 cm^{-1} in both the S_0 and S_1 states do not agree with the results derived from a fluorescence analysis. The discrepancy for a mode to which the torsion around the ethylenic C═C bond contributes greatly (ν_{35}) is particularly large and remains to be a problem to be solved in future.

References and Notes

(1) Meić, Z.; Güsten, H. *Spectrochim. Acta A* **1978**, *34*, 101.
(2) Arenas, J. F.; Tocón, I. L.; Otero, J. C.; Marcos, J. I. *J. Phys. Chem.* **1995**, *99*, 11392.
(3) Baranović, G.; Meić, Z.; Maulitz, A. H. *Spectrochim. Acta A* **1998**, *54*, 1017.
(4) Warshel, A. *J. Chem. Phys.* **1975**, *62*, 214.
(5) Meić, Z.; Baranović, G.; Skare, D. *J. Mol. Struct.* **1986**, *141*, 375.
(6) Tasumi, M.; Urano, T.; Hamaguchi, H. In *Time-Resolved Vibrational Spectroscopy*; Atkinson, G. H., Ed.; Gordon & Breach: New York, 1987; pp 252−264.
(7) Palmö, K. *Spectrochim. Acta* **1988**, *44A*, 341.
(8) Gustafson, T. L.; Roberts, D. M.; Chernoff, D. A. *J. Chem. Phys.* **1983**, *79*, 1559.
(9) Hamaguchi, H.; Kato, C.; Tasumi, M. *Chem. Phys. Lett.* **1983**, *100*, 3.
(10) Hamaguchi, H.; Urano, T.; Tasumi, M. *Chem. Phys. Lett.* **1984**, *106*, 153.
(11) Gustafson, T. L.; Roberts, D. M.; Chernoff, D. A. *J. Chem. Phys.* **1984**, *81*, 3438.
(12) Gustafson, T. L.; Chernoff, D. A.; Palmer, J. F.; Roberts, D. M. In *Time-Resolved Vibrational Spectroscopy*; Atkinson, G. H., Ed.; Gordon & Breach: New York, 1987; pp 265−285.
(13) Hamaguchi, H. In *Vibrational Spectra and Structure*; Durig, J. R., Ed.; Elsevier: Amsterdam, 1987; Vol. 16, pp 227−309.
(14) Negri, F.; Orlandi, G.; Zerbetto, F. *J. Phys. Chem.* **1989**, *93*, 5124.
(15) Weaver, W. L.; Huston, L. A.; Iwata, K.; Gustafson, T. L. *J. Phys. Chem.* **1992**, *96*, 8956.
(16) Hamaguchi, H.; Iwata, K. *Chem. Phys. Lett.* **1993**, *208*, 465.
(17) Hester, R. E.; Matousek, P.; Moore, J. N.; Parker, A. W.; Toner, W. T.; Towrie, M. *Chem. Phys. Lett.* **1993**, *208*, 471.
(18) Hamaguchi, H.; Gustafson, T. L. *Annu. Rev. Phys. Chem.* **1994**, *45*, 593.
(19) Qian, J.; Shultz, S. L.; Jean, J. M. *Chem. Phys. Lett.* **1995**, *233*, 9.
(20) Matousek, P.; Parker, A. W.; Toner, W. T.; Towrie, M.; de Faria, D. L. A.; Hester, R. E.; Moore, J. N. *Chem. Phys. Lett.* **1995**, *237*, 373.
(21) Leonard, J. D., Jr.; Gustafson, T. L. *J. Mol. Struct.* **1996**, *379*, 109.
(22) Iwata, K.; Hamaguchi, H. *J. Phys. Chem. A* **1997**, *101*, 632.
(23) Nakabayashi, T.; Okamoto, H.; Tasumi, M. *J. Phys. Chem. A* **1997**, *101*, 7189.
(24) Okamoto, H.; Nakabayashi, T.; Tasumi, M. *J. Raman Spectrosc.* **2000**, *31*, 305.
(25) Okamoto, H. *Chem. Lett.* **1998**, 1141.
(26) Okamoto, H. *J. Phys. Chem. A* **1999**, *103*, 5852.
(27) Foresman, J. B.; Head-Gordon, M.; Pople, J. A.; Frisch, M. J. *J. Phys. Chem.* **1992**, *96*, 135.
(28) Torii, H.; Tasumi, M. *J. Chem. Phys.* **1994**, *101*, 4496.
(29) Becke, A. D. *J. Chem. Phys.* **1993**, *98*, 5648.
(30) Lee, C.; Yang, W.; Parr, R. G. *Phys. Rev. B* **1988**, *37*, 785.
(31) Frisch, M. J.; Trucks, G. W.; Schlegel, H. B.; Scuseria, G. E.; Robb, M. A.; Cheeseman, J. R.; Zakrzewski, V. G.; Montgomery, J. A., Jr.; Stratmann, R. E.; Burant, J. C.; Dapprich, S.; Millam, J. M.; Daniels, A. D.; Kudin, K. N.; Strain, M. C.; Farkas, O.; Tomasi, J.; Barone, V.; Cossi, M.; Cammi, R.; Mennucci, B.; Pomelli, C.; Adamo, C.; Clifford, S.; Ochterski, J.; Petersson, G. A.; Ayala, P. Y.; Cui, Q.; Morokuma, K.; Malick, D. K.; Rabuck, A. D.; Raghavachari, K.; Foresman, J. B.; Cioslowski, J.; Ortiz, J. V.; Baboul, A. G.; Stefanov, B. B.; Liu, G.; Liashenko, A.; Piskorz, P.; Komaromi, I.; Gomperts, R.; Martin, R. L.; Fox, D. J.; Keith, T.; Al-Laham, M. A.; Peng, C. Y.; Nanayakkara, A.; Challacombe, M.; Gill, P. M. W.; Johnson, B.; Chen, W.; Wong, M. W.; Andres, J. L.; Gonzalez, C.; Head-Gordon, M.; Replogle, E. S.; Pople, J. A. *Gaussian 98*, *Revision A.9*; Gaussian, Inc.: Pittsburgh, PA, 1998.
(32) Yamakita, Y. *LXVIEW*; The University of Tokyo, 1995.
(33) Bouwstra, J. A.; Schouten, A.; Kroon, J. *Acta Crystallogr. C* **1984**, *40*, 2428.
(34) Chiang, W.-Y.; Laane, J. *J. Chem. Phys.* **1994**, *100*, 8755.
(35) Haller, K.; Chiang, W.-Y.; del Rosario, A.; Laane, J. *J. Mol. Struct.* **1996**, *379*, 19.
(36) Urano, T., Doctoral Thesis, The University of Tokyo, 1989.
(37) Tasumi, M.; Urano, T.; Nakata, M. *J. Mol. Struct.* **1986**, *146*, 383.
(38) Edelson, M.; Bree, A. *Chem. Phys. Lett.* **1976**, *41*, 562.
(39) Bree, A.; Edelson, M. *Chem. Phys.* **1980**, *51*, 77.
(40) Furuya, K.; Sakamoto, A.; Tasumi, M., manuscript in preparation.
(41) Syage, J. A.; Felker, P. M.; Zewail, A. H. *J. Chem. Phys.* **1984**, *81*, 4685. Syage, J. A.; Felker, P. M.; Zewail, A. H. *J. Chem. Phys.* **1984**, *81*, 4706.
(42) Spangler, L. H.; Zee, R.; Zwier, T. S. *J. Phys. Chem.* **1987**, *91*, 2782.
(43) Urano, T.; Maegawa, M.; Yamanouchi, K.; Tsuchiya, S. *J. Phys. Chem.* **1989**, *89*, 3459.
(44) Suzuki, T.; Mikami, N.; Ito, M. *J. Phys. Chem.* **1989**, *93*, 5124.
(45) Molina, V.; Merchán, M.; Roos, B. O. *J. Phys. Chem.* **1997**, *101*, 3478.